Geomimicry: harnessing the antibacterial action of clays

LYNDA B. WILLIAMS [*,†]

School of Earth & Space Exploration, Arizona State University, Tempe, AZ 85287-1404, USA

ABSTRACT: A decade of research on clays that kill human pathogens, including antibiotic-resistant strains such as methicillin-resistant *S. aureus* (MRSA), has documented their common characteristics. Worldwide, ~5% of clays tested to date are antibacterial when hydrated. Most antibacterial clays are from hydrothermally altered volcanics, where volcanogenic fluids produce minerals containing reduced metals. Ferruginous illite-smectite (I-S) is the most common clay mineral, although kaolins dominate some samples. Antibacterial clay mineral assemblages may contain other reduced Fe minerals (*e.g.* pyrite) that drive production of reactive oxygen species (H_2O_2, $^{\bullet}OH$, $^{\bullet}O_2^{-}$) and cause damage to cell membranes and intracellular proteins. Ion exchange can also cause loss of bacterial membrane-bound Ca^{2+}, Mg^{2+} and PO_4^{3-}.

Critically important is the role of clays in buffering the hydration water pH to conditions where Al and Fe are soluble. A nanometric particle size (<200 nm) is characteristic of antibacterial clays and may be a feature that promotes dissolution. Clay interlayers or the lumen of tubular clays may absorb reduced transition metals, protecting them from oxidation. When the clays are mixed with deionized water for medicinal applications, these metals are released and oxidized.

Different antibacterial clays exhibit different modes of action. The minerals may be a source of toxins, or by adsorption may deprive bacteria of essential nutrients. In the field, the pH and Eh (oxidation state) of the hydrated clay may help to identify potential antibacterial clays. If the pH is circum-neutral, toxic metals are not soluble. However, at pH < 5 or >9 many metals are soluble and the oxidation of transition metals increases the Eh of the suspension to >400 mV, leading to bacterial oxidation.

Understanding the antibacterial mechanism of natural clay may lead to design of new treatments for antibiotic-resistant bacteria, with potential applications in wound dressings, medical implants (joint replacements, catheters), animal feed stocks, agricultural pathogens, and production of antibacterial building materials. This research exemplifies how 'geomimicry' (copying geochemical processes) may open new frontiers in science.

KEYWORDS: geomimicry, antibacterial clay, antibiotic resistance, hydrothermal, metal oxidation.

Clays may be considered as 'healing clay' because of the many natural attributes of their nanometric mineral assemblages that are therapeutic and promote health. When consumed by humans and animals, a practice known as geophagy, the hypothesis is that the minerals provide nutrition (salt, micronutrients), soothe stomach ailments and alleviate hunger (Vermeer & Ferrell, 1985; Wilson, 2003; Ferrell, 2008, Young, 2011). Clays are also used in wound care to stop bleeding because of their capacity to adsorb fluids and protect flesh (Williams & Hillier, 2014) and have been used in pelotherapy (mud baths) for millennia (Carretero *et al.*, 2013). However, there is a subset of 'healing clays' that have been identified as antibacterial, and their properties have, only

*E-mail: Lynda.Williams@asu.edu
†George Brown Lecture, 2016, delivered at the Mid-European Clay Conference, held in Košice, Slovakia.
https://doi.org/10.1180/claymin.2017.052.1.01

recently, been investigated scientifically. This review focuses on a decade of antibacterial clay research.

The term 'antibacterial clay' must be defined carefully for the science-literate public because it draws from jargon traditionally specific to disciplines of geology, microbiology and medicine. A substance is referred to as antibacterial if it is effective at killing or inhibiting bacterial growth. However, no substance kills all bacteria, because bacteria are as diverse in function and adaptation as are humans. Species have evolved to thrive in a variety of environments, and some can tolerate extreme environments. An antibacterial agent is usually effective against a specific type or group of bacteria.

An antibiotic is a substance produced by a biological agent (fungi or other bacteria) which inhibits or kills certain bacterial species (Hoogerheide, 1944; Foster & Woodruff, 2010). However, chemicals that mimic biological substances are also called antibiotics. A 'broad-spectrum' antibiotic works against a variety of bacterial species, including Gram-negative, Gram-positive and mycobacterial species that each have different cell-membrane structures and genetic codes (Williams & Haydel, 2010). We use the term antibacterial clay, as opposed to 'antibiotic', because we are studying the inorganic reactions that affect bacteria. This is sometimes called 'geomimicry' which is the design and production of materials, structures and systems that are modelled on geological entities and processes. Clay is, of course, a size term which includes the assemblage of minerals in the <2 µm size fraction (Moore & Reynolds, 1997). By studying the processes demonstrated by natural clay deposits that inhibit or kill a broad spectrum of bacteria, one might harness the antibacterial mechanism to design new, antibacterial drugs.

This research began with the observation of an antibacterial effect of reduced-Fe bearing (green) clays from France, applied topically to treat Buruli ulcer, a necrotizing fasciitis, or 'flesh-destroying' infection (Williams *et al.*, 2004). In 2002, Line Brunet de Courssou, a French philanthropist, travelled to the Cote d'Ivoire (Africa) on a humanitarian mission and observed many woman and children of the local tribes suffering from Buruli ulcer. This infection was first described by Sir Albert Cook in patients from Buruli County in Uganda, and the causative organism, *Mycobacterium ulcerans*, which is related to leprosy and tuberculosis, was isolated in 1948 by MacCallum in the Bairnsdale region of Victoria, Australia (WHO, 2008). George *et al.* (1999) first isolated a toxin called mycolactone, produced by *Mycobacterium ulcerans* and showed that it was responsible for the infection.

Women and children of the tribes investigated near Zouan Hounein (Cote d'Ivoire) are the primary 'food-gatherers' and often forage in the swamplands of the country. Certain aquatic insects (*e.g.* Naucoridae) have been found to harbour *Mycobacterium ulcerans* in glands of their pincers (Marsollier *et al.*, 2002; Portaels *et al.*, 2008). It is believed that bites from these insects that live near roots of swampy plants, provide a vector for transmission of this bacterium. The *Mycobacterium ulcerans* are slow to grow; doubling their population *in vitro* takes nearly one month. Those bitten by the insect might not notice an infection for months to years after the bacteria are transmitted to the skin.

Line Brunet de Courssou treated people with Buruli ulcer using poultices (hydrated clays) of French Green clay from two different suppliers in France (Argicur and Argiletz). She studied carefully their response to daily application of the clay poultices, with photographic documentation of healing the infection (Fig. 1). At the time there was no antibiotic that cured Buruli ulcer, and the most effective treatment was excision or amputation of the infected limbs. After one day of applying the Argiletz clay in hydrated form, the skin tissue was debrided with complete removal of necrotized tissue. The treatment was painful for the first week, but pain lessened as the open wounds healed (Brunet de Courssou, pers. comm.). Brunet de Courssou observed that the edges of the skin became purple, which is a pathological response to extraneous materials that become deposited in the skin or deeper tissues. When this occurred she changed to the Argicur clay, and healing proceeded over a period of several months. The healing returned the skin to a soft, supple state, with minor scarring, and returned mobility to affected joints.

Brunet de Courssou provided samples of the two French green clays she used so that we could test their mineralogical and geochemical compositions. She hypothesized that the clays might contain fibrous illite that could physically damage bacterial cells. However, scanning electron microscopy imaging of the French green clays showed that both the Argiletz and Argicur clays contained small (∼200 nm) hexagonal illite (Fig. 2). This led to our first investigation of the antibacterial effectiveness of clays (Williams *et al.*, 2008). The World Health Organization could not help fund the treatment of Buruli ulcer with clays until there was some basic understanding of what makes the clay treatment effective. This required interdisciplinary studies of clay mineralogy, geochemistry, microbiology and medicinal response to the clay application.

Fig. 1. Photo-documentation (by Thierry Brunet de Courssou) showing the gradual healing of Buruli ulcer infection by daily application of hydrated French green clay (modified from Williams *et al*., 2004).

INVESTIGATING ANTIBACTERIAL CLAYS

The approach taken to investigate the observed antibacterial action of the French green clays was to first evaluate the effectiveness of various clay samples *in vitro* against a broad spectrum of human pathogens (Haydel *et al*., 2008). The bacteria tested included common and antibiotic-resistant strains of human pathogens: *E. coli* (ATCC 25922), Extended Spectrum Beta Lactamase (ESBL)-resistant *E. coli* (ATCC 51446), *Salmonella enterica serovar Typhimurium* (ATCC 14028), *P. aeruginosa* (ATCC 27853), *S. aureus* (ATCC 29213), Methicillin-resistant *S. aureus* (MRSA; from Sonora Quest Laboratories; resistant to ten antibiotics; Haydel *et al*., 2008), *Mycobacterium smegmatis* (ATCC 19420), *M. marinum* (ATCC 927) and *M. ulcerans*. With the exception of the mycobacterial strains tested, the Clinical Laboratory Standards Institute (CLSI) recommends these bacteria as quality control strains for laboratory testing of antimicrobials.

Next, we determined the mineralogical composition of the French green clays to compare with their antibacterial effectiveness (Williams *et al*., 2008). We hypothesized that the bacteria are killed when exposed to hydrated clays either by a physical attack or by chemical transfer. It has been shown (Konhauser & Urrutia, 1999; Wei *et al*., 2011) that clay minerals can adhere to bacteria by physical attraction to the bacterial membranes; enveloping them may block the uptake of nutrients and expulsion of waste products. In fact, clays can be modified to have such a large surface energy that they can kill bacteria by physically tearing cell membranes (Rossman Geise, SUNY Buffalo, pers. comm.). However, none of the antibacterial clays we have tested kills by physical destruction. Alternatively, we consider that the clays may rob bacteria of nutrients, by competition of ions for exchange sites on clay surfaces, or that the clay mineral assemblage provides

toxins that overwhelm the regulatory systems of the bacteria. For example, lipid peroxidation of bacteria by oxidative stress induced by Fe-smectites has been documented (Kibanova *et al*., 2009).

Physical or chemical interactions

One can measure the zeta potential of the clay and bacteria to test for physical interactions. When dealing with clay mineral assemblages, the zeta potential can be quite variable because it is an average of the multi-mineral suspension. Isolating each mineral component of the assemblage might bias the results; therefore we test the natural assemblage. Furthermore, it is important to simulate the chemistry of the fluid equilibrated with the mineral assemblage in order to evaluate the surface energy in the hydrated medium. Because the antibacterial clays from France were changed daily, we infer that the antibacterial process occurs within 24 h, therefore the antibacterial clay assemblage was consistently equilibrated for 24 h with deionized
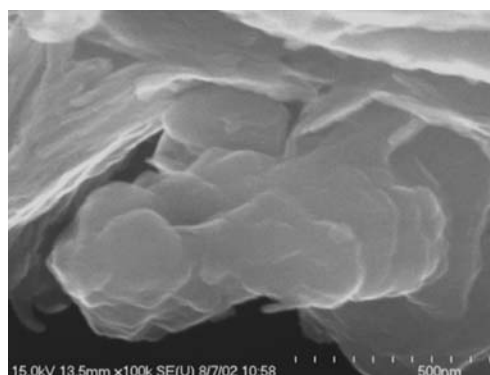

Fig. 2. SEM image of the Argicur French green clay used by Line Brunet de Courssou to treat Buruli ulcer patients. The illite forms small hexagonal plates ~200 nm in diameter (photo by L. Williams).

water (DIW) for our experiments. This produces an ionic strength appropriate for the zeta potential measurement. The measurements are taken over a range of pH in order to evaluate the energy changes resulting from attraction of H^+ or OH^- to the mineral or bacterial surface. An example is given later for a Colombian Amazon clay (AMZ) that kills human pathogens (*E. coli, B. subtilis*).

Another way to test for a physical effect of clay on bacteria is by isolating the two populations. We have suspended autoclaved (sterilized) clays (500 mg/mL) in a beaker and submerged dialysis tubes (with 25 kDa molecular weight cutoff) containing *E. coli* (ATCC 25922) in log phase growth, in the beaker of suspended clay (Williams *et al.*, 2011). This allowed diffusion of elements from the hydrated clay into the bacterial suspension. After 24 h of incubation at 37°C the viability of the bacteria was tested by live/dead cell epifluorescence staining (Invitrogen; Thermo Fisher Scientific L7007). Antibacterial clays completely killed bacteria (red stained), compared to cells not exposed to the clay (green). This verified that no physical contact between the clay and bacteria was required. The bacteria were killed either by a chemical transfer of toxins to the bacteria, or loss of nutrients absorbed by the clay.

Bacterial viability testing

Standard antibacterial susceptibility testing (CLSI, 2015) was used for evaluating the effectiveness of natural clays in killing or inhibiting the growth of bacteria. Antibacterial minerals that completely kill a particular bacterial population are called bactericidal, whereas those that inhibit reproduction are called bacteriostatic. Clay that reduces the bacterial population by several orders of magnitude, compared to an untreated bacterial population, is called inhibitory. Once we identify a clay that is antibacterial we then determine the minimum inhibitory concentration (MIC), defined as the concentration that reduces a bacterial population by 50% compared to an untreated control population; and 'minimum bactericidal concentration' (MBC), defined as the concentration that kills 99.9% of the bacteria (Amyes *et al.*, 1996).

The clay size fraction (<2 µm) is separated (Moore & Reynolds, 1997) without cation exchange in order to preserve interlayer cations that may be important sources of dissolved metals. This procedure requires rinsing of salts from the sample until the clays are dispersed; therefore the sample is washed of surface components, and then dried. The dried clay sample is autoclaved (121°C; 1 h) to kill any inherent (environmental) or airborne bacteria that may settle on the sample. For initial testing, a suspension is made of 200 mg of clay in 400 µL of DIW (deionized water). The dose varies if the clay has significant smectite and forms a gel. The suspension must be dilute enough to be easily pipetted into the bacterial suspension. Bacteria are grown in a suspension in their growth media (*e.g.* Luria Broth; LB) at body temperature (37°C) and their numbers are measured by colony-forming units (CFU) per mL of suspension. We start with bacteria in their 'exponential' or 'log phase' growth ($\sim 10^7$ CFU/mL), which is when they are at their healthiest life stage. When bacterial populations are too dense they reach 'stationary phase' where the population begins to die and the number of new bacteria equals the number of dead bacteria. Therefore, an overabundance of CFU is avoided by diluting the bacterial population with fresh growth media. Finally, the clay suspension (in DIW) is mixed with the bacterial suspension (in liquid growth media) in a 1:1 ratio, and incubated overnight (37°C) on a rotational shaker to keep the solids suspended. Serial dilutions of the incubated suspension are made according to CLSI (2015) procedures, diluting the mixture by orders of magnitude (to 10^{-8}). Each dilution is spread evenly on agar plates (petri dishes) containing the growth media, and incubated again for 24 h, allowing the bacteria that were not damaged by the clay to grow (Fig. 3). A positive control population of the bacteria is grown in the absence of clay for comparison to the population incubated with the clay suspension. In addition, a control bacterial population is tested with standard reference clay minerals (Source Clays Repository, The Clay Minerals Society) of the dominant clay mineral in the natural sample (*e.g.* IMt-1 illite, SWy-1 smectite, KGa-1 kaolinite), none of which has shown antibacterial effects. The SWy-1 (Wyoming bentonite) increases bacterial growth compared to the control grown without clay (Williams *et al.*, 2004), possibly by providing additional nutrient. The agar plates that show growth of bacterial colonies after 24 h of incubation are counted, with counts adjusted for the dilution factor. Experiments are always performed in triplicate (three separate preparations of the clay-bacteria mixtures), for statistical evaluation. The example (Fig. 3) comparing the antibacterial effects of the French green clays shows that the clay supplied by Argicur completely killed *E. coli*, whereas the Argiletz-supplied clay, and the comparable Fe-bearing illite Muloorina, did not. The geochemical differences between the French green clays are discussed later.
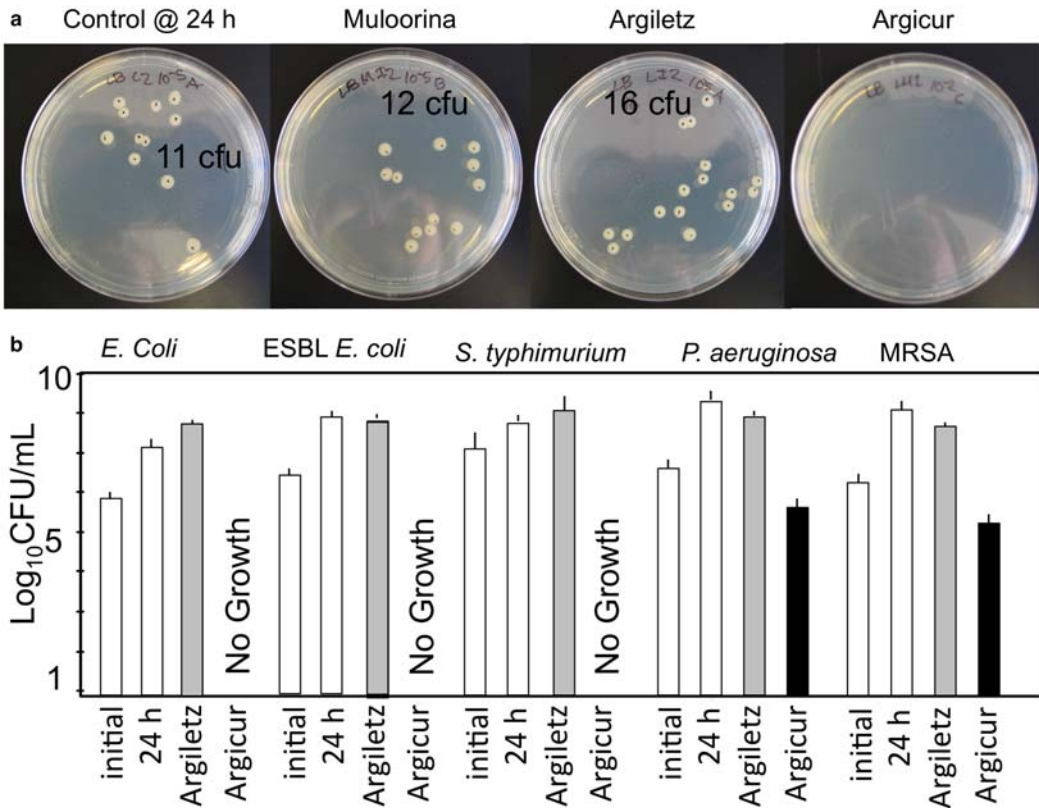
Fig. 3. Antibacterial susceptibility is determined by plate counting (CLSI, 2015). (a) Serial dilutions of *E. coli* incubated (37°C) with clay suspensions (24 h) are compared to control *E. coli* grown without clay. (b) Bar graphs showing CFU for a variety of human pathogens tested compared to controls showing the initial and 24 h counts of bacteria without clay (control). All experiments were performed in triplicate using three separate preparations of the clay-bacteria suspensions.

The bacteria grown in their particular growth media (*e.g.* LB) is a standard microbiological method for evaluating antibacterial agents but it does not represent the geochemical conditions of a topical application of hydrated clay to the bacteria growing in wounds. In particular, if there is chemical transfer of an element derived from the clay through water to affect the bacteria, then the presence of bacterial nutrients in growth media (organic compounds, salts) will change the aqueous speciation of the fluid. Therefore, we further tested the effect of French green clays on bacteria in normal saline (8.5% NaCl; isotonic solution) needed to prevent bacteria dying from osmotic shock. In every test the results show some depletion of the bacterial population due to the lack of nutrition, but dramatic killing of the bacterial

populations when antibacterial clays are present (Morrison *et al.*, 2014; Londoño & Williams, 2016).

Aqueous leachates of the clays were prepared by equilibrating the clay with water (shaken together at 50 mg clay/mL DIW) for 24 h; again the reaction time was chosen to simulate the topical application of the hydrated clay poultice, which was changed daily. Elemental analyses of the leachates were conducted using inductively coupled plasma-mass spectrometry (ICP-MS) (USGS, Boulder, Colorado, USA), to look for high concentrations of known toxic elements (*e.g.* Ag, Cu, Cd, Se, Hg, As) and to determine differences in the elements derived from the two French green clays (Williams *et al.*, 2008). Furthermore, cation exchange of the clay using 1 M KCl (Na, Ca and NH_4^+ salts were also tested) removed

TABLE 1. Broad-spectrum antibacterial effectiveness of the four antibacterial clays tested. The percentage of bacteria killed is indicated for variable incubation times, all at 37°C. Initial bacterial populations were in log phase growth.

Bacterial species	Time	Argicur	Argiletz	OMT	Walker
Escherichia coli (ATCC 25922)	24 h	100%	0%	100%	100%
ESBL E. coli (ATCC 51446)	24 h	100%	0%	100%	100%
Salmonella e.s. typhimurium (ATCC 14028)	24 h	100%	0%	100%	100%
Pseudomonas aeruginosa (ATCC 27853)	24 h	100%	0%	100%	100%
Staphylococcus aureus (ATCC 29213)	24 h	92.7%	0%	100%	99.1%
Staphylococcus epidermidis (ATCC 14990)	24 h	n.a.	n.a.	100%	n.a.
M.R.S. epidermidis (ATCC 35948)	24 h	n.a.	n.a.	100%	n.a.
M.R.S. aureus (Sonora Quest Labs)	24 h	84%	0%	100%	99.5%
Mycobacterium smegmatis	48 h	96.8%	0%	n.a.	n.a.
Mycobacterium marinum	5 days	100%	0%	n.a.	n.a.
Mycobacterium ulcerans	28 days	99.5%	0%	n.a.	n.a.

All experiments performed in triplicate.
n.a. = not analysed.

the exchangeable cations and the Argicur clay still proved to be antibacterial.

The results of the variable effectiveness of *in vitro* testing of the two French Green clays used in the treatment of Buruli ulcer (Fig. 3) show that Argicur sourced clay completely killed the Gram-negative bacterial pathogens tested, and inhibited the Gram-positive *P. aeruginosa* and methicillin-resistant *S. aureus* (MRSA) by three orders of magnitude. In contrast, the Argiletz-sourced clay had no effect on the bacteria tested, within statistical uncertainty. Interestingly however, both clays were effective against *M. ulcerans* (Table 1).

FRENCH GREEN CLAYS

Mineralogy

The mineralogy of the green clay from the Argiletz (supplied in 2002) and Argicur (supplied in 2002) samples (Fig. 4) used by Brunet de Courssou in the Cote d'Ivoire, is dominated by two phases of illite, one disordered (1*Md*), and a 1*M* illite-smectite with R2 ordering. Fe-rich smectite is second in abundance, comprising up to 35 wt.% of the Argicur. The non-clay phases in common include feldspars, micas and quartz. The one mineral that distinguishes the antibacterial
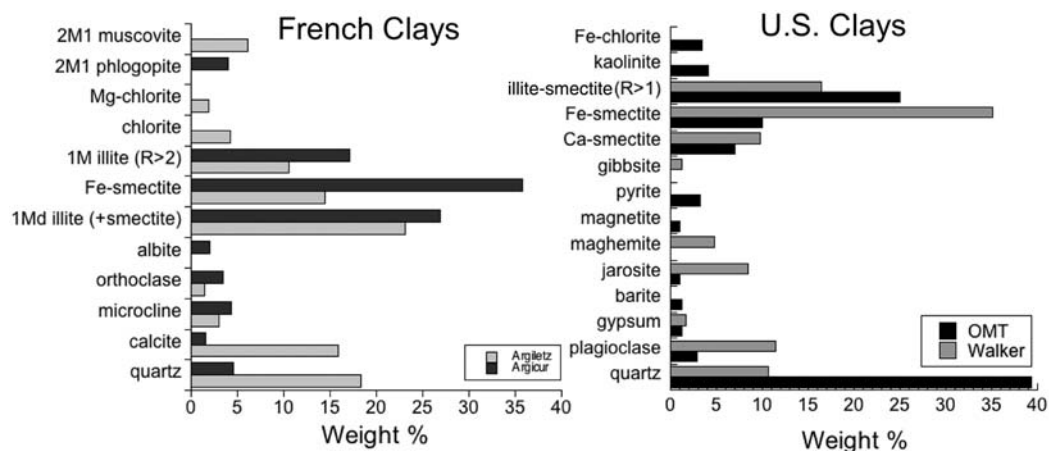

FIG. 4. Mineralogical comparisons of the two French clays and two US antibacterial clays. The mineralogy was determined by X-ray diffraction (Cu-*K*α) on bulk powders, using *RockJock* (Eberl, 2003) for quantification.

TABLE 2. Chemical analyses (µg/mL) of aqueous leachates from antibacterial clays discussed in this review.

Mass/Element	Argicur	Argiletz	OMT	Walker	AMZ
7/Li	2.8	0.7	0.6	0.2	n.a.
9/Be	n.a.	0.0	0.1	0.1	n.a.
11/B	9.6	2.6	0.0	0.1	n.a.
23/Na	3720	174	67	102	306
24/Mg	12.4	60.4	1128	101	200
27/Al	101	19	5048	362	8
28/Si	148	86	28.6	71.2	n.a.
31/P	8.9	1.2	278	3.0	5.3
39/K	154	246	35	62	1011
44/Ca	70	446	6618	4900	480
47/Ti	0.94	0.18	1.0	0.4	b.d.l.
51/V	0.43	0.057	2.0	0.02	0.5
52/Cr	0.026	0.010	1.0	0.012	b.d.l.
55/Mn	1.1	0.119	46	12	46
56/Fe	5.6	12.5	18030	5	0.6
59/Co	0.002	0.003	11.0	0.7	1.2
60/Ni	0.088	0.022	12.0	0.6	1.2
63/Cu	0.054	0.044	12.0	3.0	15.1
66/Zn	0.1	0.1	4.0	2.0	11.9
69/Ga	0.0028	0.0176	0	0	n.a.
72/Ge	n.a.	0.0004	0	0	n.a.
75/As	5.2	0.0182	2	0.01	b.d.l.
77/Se	0.03	0.12	0.2	0.01	5.3
85/Rb	0.36	0.129	0.2	0.10	1.5
88/Sr	1.2	10.4	27.0	5.0	7.0
89/Y	0.0060	0.0112	1.3800	0.1200	b.d.l.
90/Zr	n.a.	0.0190	0	0.0060	b.d.l.
93/Nb	0.0003	0.0004	0	0.002	b.d.l.
95/Mo	0.1564	0.0130	0.2000	0.0080	b.d.l.
109/Ag	0.0048	0.0001	0.0002	0.0020	b.d.l.
208/Pb	0.0052	0.0085	0.004	0.002	b.d.l.
232/Th	0.0040	0.0033	0	0.0040	b.d.l.
238/U	0.9800	0.0182	0.0030	0.0600	b.d.l.
pH	10.2	7.6	4.2	4.0	4.3
Eh (mV)	230	258	611	380	361

Analyzed by ICP-MS, 50 mg clay/mL DIW, equilibrated for 24 h. Analyses calibrated using the EPA method 3050B (EPA, 1996) with the average of triplicate analyses reported having relative standard deviations of <10%.
n.a. = not analysed.
b.d.l. = below detection limit.

Argicur green clay from the non-antibacterial Argiletz green clay is calcite. Calcite makes up >15 wt.% in the Argiletz, reflecting the circumneutral pH (7.6) buffered by that clay assemblage, where calcite is stable. However, the antibacterial Argicur clay buffers the hydrated clay suspension (50 mg/mL) pH to 10.2 where Al, in particular, is soluble. We have found that all of the antibacterial clays buffer aqueous suspensions to <5 and >9, where Al is soluble, and we infer that transition metals may also be released by aluminosilicate dissolution.

Size matters

The role of mineral dissolution as a source of toxic elements in the antibacterial process is supported by the observation that particle size influences the antibacterial effect. Only the <0.2 μm size fraction of Argicur is antibacterial (Williams *et al.*, 2008). Detrital minerals (quartz, feldspar) dominate the coarser size fractions that are not antibacterial. Furthermore, most of the illitic crystals (illite-dominated I-S) in the <0.2 μm fraction of the Argicur are ~200 nm in diameter (Fig. 2). In fact, this small dominant crystal size is common to all of the antibacterial clays we have studied to date. The larger relative surface area of small particles leads to more interaction with water, increasing the hydration of exchangeable metals, and also increasing the likelihood of mineral dissolution as the addition of DIW changes the equilibrium (*e.g.* ionic strength) of the clays taken out of their depositional environment. It has been shown that smectite dissolution occurs from edge sites of the mineral in alkaline solutions (Yokoyama *et al.*, 2005). In particular, oxidation reactions will occur that might particularly affect reduced Fe-smectite. Given the high pH (>10) of the Argicur clay, when equilibrated with DIW, it is likely that some smectite dissolution occurs.

Geochemistry

The geochemistry of the two French green clays (Williams *et al.*, 2008) differs even though the mineralogy of the two clays is very similar. Both clays contain 5–6 wt.% Fe in I-S. The amount of Fe is larger in the <0.2 μm size fraction as that is where the Fe-smectite and illite phases are concentrated. However, the aqueous leachates of the clays differ, particularly in terms of Al content, which is >100 μg/mL in the leachates equilibrated (24 h) with the anti-bacterial Argicur clay (Table 2). The amount of known toxins such as Cu, Ag and Pb are all below the MIC reported for the model bacteria tested (Nies, 1999).

Argicur Inc. (http://www.lebuissondecadouin.fr/annuaire/argicur/) could not reveal the geological source of the green clay used by Brunet de Courssou in the treatment of Buruli ulcer. All of their clay products were sampled and tested again in 2005, including the stockpile of green clay that was used for Buruli treatments and provided for our testing in 2002. However, none of the 2005 samples showed any antibacterial effect, even though the original samples provided to us in 2002 are still antibacterial. Two possible reasons for this are proposed. One is that the

clay stockpile was outdoors, exposed to precipitation for 5 y, which probably oxidized the clay (although it was still green in colour). In addition, chemical additives (*e.g.* NaHCO$_3$) were applied to the clay to increase its heat capacity for use in spas, and may have altered the interlayer chemistry, removing important exchange cations, altering the surface energy of the clay, and changing the pH, all of which may have eliminated the antibacterial effect.

U.S. ANTIBACTERIAL CLAYS: HYDROTHERMAL DEPOSITS

Without knowing the geological/depositional environment of the antibacterial French green clay, we attempted to identify other antibacterial clays that might provide accessible depositional environments to study. A survey of on-line 'healing clays', clay repository standard reference clays, and dozens of samples from oil companies, clay industries world-wide, and private land owners showed only ~5% that were antibacterial. One particular Blue clay deposit from Douglas Co., Oregon (USA) was the most effective antibacterial clay we have found, killing 100% of the broad-spectrum of bacteria tested (Table 1), including antibiotic-resistant strains (Morrison *et al.*, 2016). Rogue Silicates Inc. leases the mineral rights to the deposit, and Oregon Mineral Technologies (OMT) developed the deposit. OMT supported our study of the depositional environment of their antibacterial clay by allowing access and facilities for the field work.

Another antibacterial clay was identified from the Walker Lake region of Nevada. This clay was originally marketed by Miraculite LLC, and has been sold as a dietary supplement for Fe under the name SierraSil®. We have not studied this clay depositional environment, but the location, mineralogy and anti-bacterial effect were comparable to the results for the Oregon Blue clay. In this text we refer to the Nevada deposit as the Walker clay. Table 1 compares the antibacterial effects of the OMT and Walker clays on a broad spectrum of bacterial pathogens. Both are antibacterial at the concentration tested (100 mg/mL), but the OMT is more effective against MRSA.

Mineralogical comparison

The mineralogy of these two US antibacterial deposits (Fig. 4) shows that mixed-layered illite-smectite dominates these clays, and they also contain discrete Ca- and Fe-smectites, minor kaolinite and chlorite. Like the French green clays, the deposit
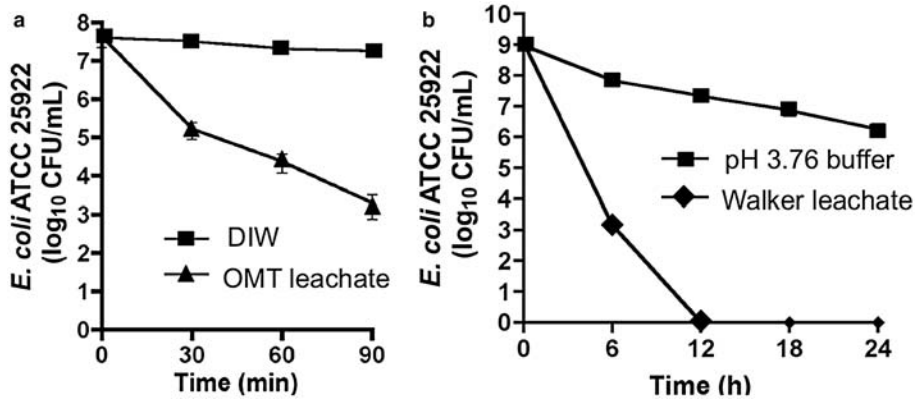
FIG. 5. Antibacterial effect of aqueous leachates on *E. coli* over time comparing: (a) OMT to DIW; and (b) Walker to DIW buffered at pH 3.76, the pH of the leachate. The rapid decline in bacteria treated with leachates compared to water alone and bacteria in acidified water indicates that pH alone is not killing the *E. coli*.

contains considerable feldspar and secondary quartz from the hydrothermal alteration of andesite porphyry (Morrison *et al.*, 2014). Of importance are minor amounts of reduced Fe-bearing phases including pyrite, magnetite and maghemite. The presence of gypsum indicates a sulfate-rich environment consistent with magmatic fluid inputs from the primary igneous source (Morrison *et al.*, 2014).

The aqueous leachates of the OMT and Walker clays are both antibacterial (Fig. 5). However the OMT leachate completely kills model *E. coli* (ATCC 25922) within 90 min, while the Walker leachate takes 12 h. The chemistry of the aqueous leachates of these clays (Table 2) shows that both are high in Mg, Al and Ca,

but the OMT leachate is extraordinarily high in Fe. This supports the conclusion that the aluminosilicates containing reduced Fe, and possibly other transition metals, seem to be involved in the antibacterial effectiveness. Therefore, we mapped the mineralogical and geochemical properties of the various clay alteration assemblages found in the OMT deposit and compared their antibacterial effectiveness (Morrison *et al.*, 2014; Morrison 2015).

Oregon blue clay

The OMT deposit is located ~30 km west of Crater Lake, Oregon (Fig. 6), but it is associated with
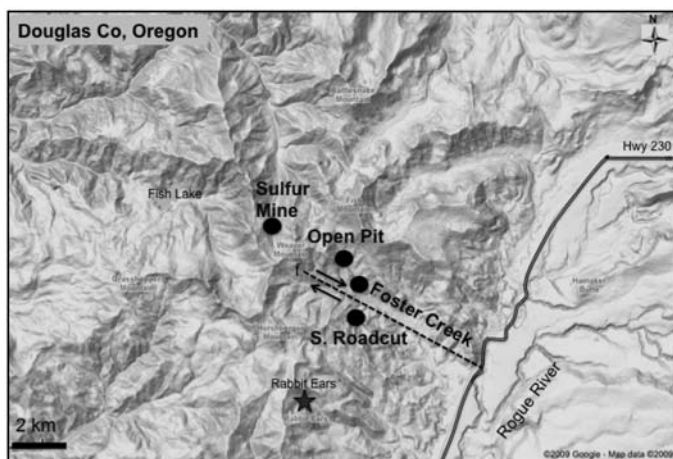

FIG. 6. Field area of the Oregon Mineral Technologies deposit and major sites sampled.

FIG. 7. Clay alteration assemblages studied in the OMT deposit. (a) Blue clay, (b) White clay in fault zones, (c) Black clay rich in pyrite, (d) Red oxidized surface clay found at all locations and elemental sulfur from the Sulfur mine location (photos by K.D. Morrison, 2015).

volcanics that are ~30 Ma older than the eruption of Mt. Mazama that formed Crater Lake (Bacon & Nathenson, 1996). The dominant host rock of the region is a porphyritic andesite, capped by younger basalts. A major fault runs NW–SE through the region focusing drainage down the Foster Creek, which drains into the N–S trending Rogue River. The OMT Blue clay is exposed in several areas across this valley, and deeper (hotter) parts of the deposit are found to the NW where sulfur was mined in the 1900s. An open pit mine exposed the relationship of several clay alteration zones in this deposit. The dominant Blue clay is a hydrothermal alteration product of the andesite porphyry that contains 4–6 wt.% pyrite. Beneath this, exposed primarily in the Sulfur mine region, is a Black clay that has large amounts of pyrite (~9 wt.%) intermixed with Blue and White clays, with large crystals of elemental sulfur precipitated in late (cooling) stages of the hydrothermal alteration (Fig. 7). The faults that run through the open pit and

regionally trend NW–SE are associated with White clays bearing smectite, but no pyrite. These 'bleached' clays are interpreted to have formed from meteoric water percolating through the faults as the system cooled (Morrison et al., 2014; Morrison, 2015). Red clays at the surface contain goethite from oxidation of the pyrite-rich Blue clays.

Regional antibacterial testing

For rapid assessment of large numbers of clay samples it was not practical to perform antibacterial susceptibility by plate counting. Instead, Kirby-Bauer disk diffusion methods were modified (Bauer et al., 1966) for antibacterial mineral mapping. Using model E. coli (ATCC 25922) grown in agar with LB growth media (10 g LB/mL), 8 mm round wells perforating the agar (4 mm deep), were filled with hydrated clays (100 mg/mL) and incubated at 37°C for 24 h. The diffusion of elements into the bacteria creates a 'zone
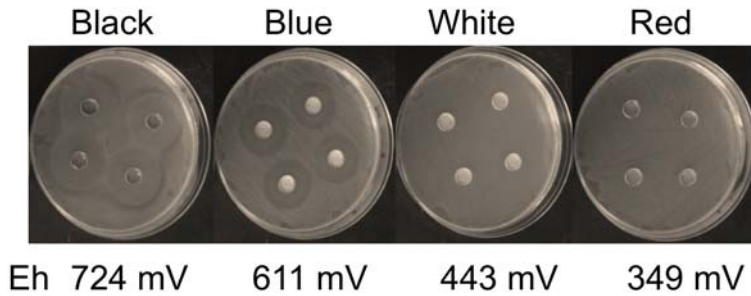
F<small>IG</small>. 8. Zones of *E. coli* growth inhibition by disk diffusion away from hydrated clays taken from the major alteration assemblages identified in the OMT deposit.

of growth inhibition' around the wells, and, by measuring the diameter of the inhibited growth zone, one can approximate the antibacterial effectiveness. An example of the disk diffusion method (Fig. 8) is shown for the four major clay alteration zones. The Black clay containing the most pyrite shows the greatest antibacterial effect and the Red oxidized clay shows no zone of inhibition.

Mineralogy

Quantitative mineralogy was determined by X-ray diffraction on random bulk powders of the clay samples using alumina as an internal standard and *RockJock* 11 interpretive software (Eberl, 2003). Table 3 shows the bulk powder mineralogy for each of the major clay alteration zones. This comparison shows that the most antibacterial zones (Black and Blue) contain pyrite; however, the White clay also inhibits bacterial growth, but does not contain detectable amounts of pyrite. Notably, the White clay contains variable amounts of smectite, which may act as a reservoir for reduced Fe released from pyrite that may have dissolved during the bleaching process (meteoric water percolation). Other important observations are that the Blue and White zones contain gypsum, indicative of the oxidation of sulfides. The Red clay contains goethite, indicating the complete oxidation of Fe^{2+} to Fe^{3+}, and calcite indicating that the pH must be >7. The pH and Eh (average values) for each clay zone are noted at the bottom of Table 3. As a reminder, these values were measured on the clay after hydration with DIW at the constant ratio of 50 mg clay/mL, equilibrated for 24 h. The pH of the clay suspension increases from ~2 in the Black clays deep in the hydrothermal system to ~7 in the Red clay at the surface. Conversely, the Eh decreases from >700 mV in the Black clay to ~350 mV in the surficial Red clay.

X-ray diffraction patterns of the ethylene glycol-saturated, oriented, clay-size (<2 µm) fraction from the various alteration zones of the OMT deposit (Fig. 9) were interpreted using *Sybilla* (Zeelmaekers *et al.*, 2009). As shown by the bulk powder XRD, the dominant clay minerals in each alteration zone are I-S, but the %I and I-S ordering vary, primarily reflecting temperature variations. The most abundant clay is rectorite in the Blue clay alteration zone, an R1 ordered I-S with 55%I (Morrison *et al.*, 2014). Other outcrops of the Blue clay have 70%I in I-S plus discrete smectite, with up to 85%I, R3 ordered I-S in a road-cut exposure south of the open pit indicating higher temperatures. The Black clay from the Sulfur Mine

T<small>ABLE</small> 3. Bulk mineralogical composition of the four alteration zones in the OMT deposit (wt.%).

Mineral	Black	Blue	White	Red
Non-clays				
quartz	11.3	42.2	50.0	36.3
plagioclase	4.8	2.5	3.0	4.6
pyrite	9.0	3.1		
sulfur	47.0			
gypsum		1.2	2.8	
goethite				3.4
calcite				2.8
Clays				
illite-smectite	27.8	51.1	37.7	44.6
smectite		6.5		
kaolinite				4.7
chlorite				3.5
pH[a]	2.0	2.9	4.2	6.9
Eh[a] (mV)	724	611	443	349

[a] 50 mg clay/mL DIW equilibrated for 24 h.
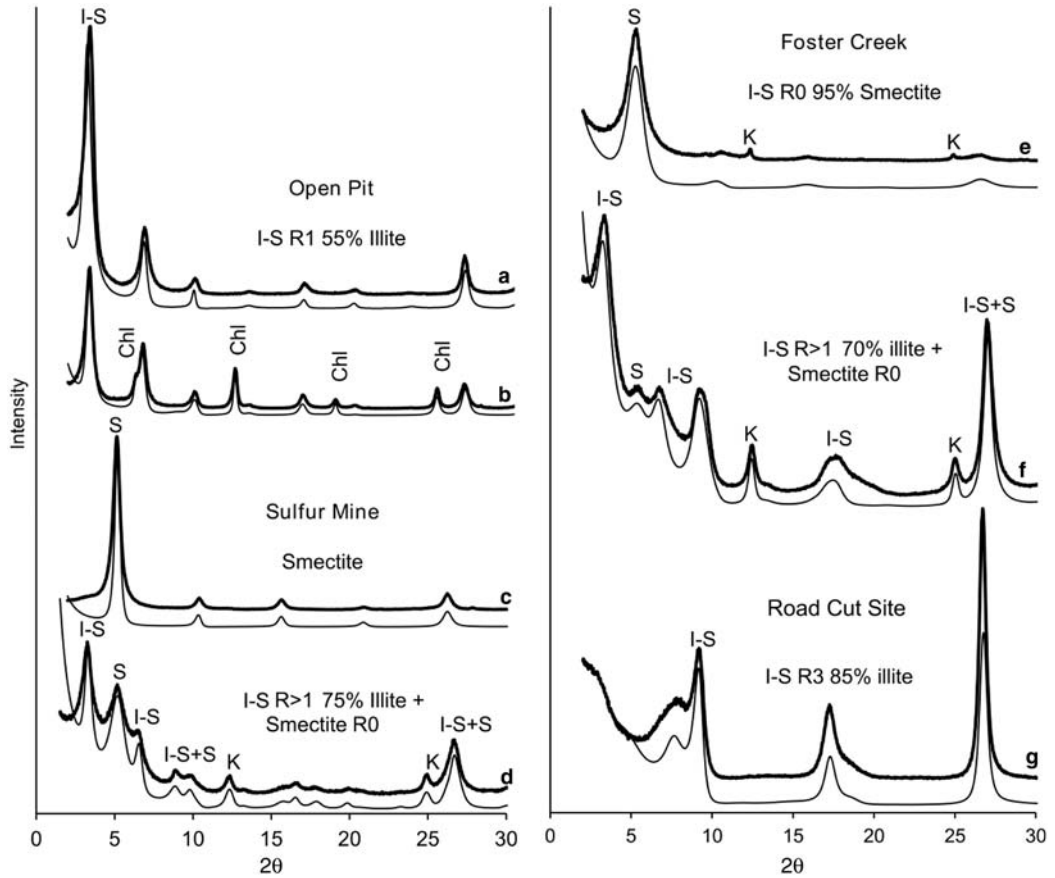
FIG. 9. XRD patterns of oriented, ethylene glycol-saturated <2 μm size fraction separates from (a) Open Pit Blue clay, (b) Open Pit perimeter, (c) Sulfur Mine White clay, (d) Sulfur mine Blue clay, (e) Foster Creek White clay, (f) Foster Creek Blue clay, (g) Roadcut Blue clay (Sample locations in Fig. 6; data from Morrison, 2015).

region contains 70%I in I-S (R > 1). Finally the White clay, associated with fault traces, grades from pure smectite where the fluid:rock ratio is high, and temperatures relatively low, to more I-S approaching the country rock that experienced higher temperatures through hydrothermal alteration. Some regions exhibit minor kaolinite and chlorite.

It appears that a combination of the clay minerals, which serve as the dominant pH buffer for fluids, and phases that contribute reduced Fe (*e.g.* pyrite) or other redox reactive metal, act to create an antibacterial mineral assemblage. There are two forms of pyrite in this deposit; one is a crystalline pyrite with crystals >10 μm in diameter and the other is sub-micron spherical pyrite physically intermixed with clay minerals (Fig. 10). Figure 11 shows a high-resolution SEM image of the Blue clay containing small

rod-shaped features (1 μm long) that look like bacteria. These bodies have concentrated Fe and S according to EDX-ray maps, and supported by NanoSIMS ion imaging (data not shown). RNA was extracted from the inherent environmental bacteria found in fresh samples taken from the Blue clay in the open pit and 19 nucleotide sequences of the taxa were analysed for genetic evolutionary relationships (Weimin Gao, Arizona State University Biodesign Institute, USA, pers. comm.). The dominant environmental bacteria living in this clay are from the genus *Burkholdaria* with 12 taxanomic subunits. These are CO-oxidizing, mixotrophic acidophiles common in volcanic soils (King *et al.*, 2008; Weber & King, 2010) and some species are known to accumulate Fe aggressively (Kvitko *et al.*, 2012). These environmental microbes may provide nucleation sites for accumulation of the
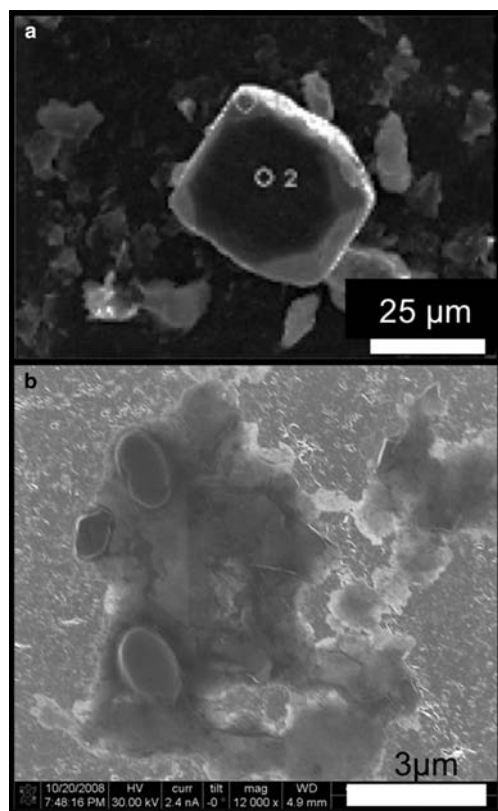
FIG. 10. Pyrite morphologies in the OMT Blue clay alteration assemblage. (a) Crystalline pyrite is >10 μm across, whereas (b) <1 μm Fe-S-bearing spheres are abundant in the clay matrix (Williams *et al.*, 2011).

sub-micron pyrite that is more soluble under oxidizing conditions than the larger crystalline pyrite, and may contribute to the large amount of Fe^{2+} in the Blue clay aqueous leachate.

Oxidation states of minerals and hydration water

Important information about the antibacterial process was derived from sampling the Blue clay in the open pit mine, with depth from surface (Fig. 12). Samples were taken at intervals down to 1.5 m and their mineralogy, geochemistry and antibacterial effectiveness were compared. Samples were also taken from the surficial Red clay, a fault zone containing White clay, and the stockwork veins of quartz and pyrite that underlie the deposit (Morrison, 2015). The antibacterial effectiveness of each sample was determined using 100 mg clay/mL, which was

determined by plate counting to be the MBC. Samples from the surface-oxidized Red clay showed no antibacterial effect, as expected. However, within the Blue clay the antibacterial effect decreased with increasing burial depth. This was an unanticipated trend, given that the Black clay from the Sulfur Mine which contained 9 wt.% pyrite was the most antibacterial (produced the largest zone of inhibition; Fig. 8). Within the Blue clay, Morrison (2015) found the greatest antibacterial effect in samples with higher oxidation states (Eh up to 725 mV). His work shows that it is not the amount of pyrite in the clay, but rather the oxidation state of the hydrated pyrite-bearing clay that drives the antibacterial process. The samples deeper in the pit are less oxidized, with Eh values closer to 400 mV, and are less thus effective at killing bacteria. Presumably, these deeper samples would be more effective antibacterial agents as they become more oxidized (surface exposure over time, or by addition of dissolved O_2).

The White clay from the exposed fault (Fig. 12) contains no pyrite, but it is inhibitory to bacterial growth (pH ≈ 4.2; Eh ≈ 450). Samples from the stockwork veins composed primarily of hydrothermal quartz and crystalline pyrite are not antibacterial. Although pyrite is a source of dissolved Fe^{2+}, it appears that the more crystalline forms (>10 μm) are not soluble enough to provide a sufficient supply of Fe^{2+} to kill *E. coli*. We hypothesize that the presence of expandable clay minerals (I-S) is important for buffering the pH to conditions where Fe^{2+} is soluble from the sub-micron pyrite, and potentially the clays stabilize Fe^{2+} in their interlayers, which act as a reservoir of the reduced Fe that is released upon addition of DIW. In other words, the expandable clays may act as a capsule for extended release of antibacterial agents. What is most important is the oxidation state during the reaction of Fe^{2+} to Fe^{3+}. In the Red clay, the oxidation state of the minerals reaches >800 mV, where Fe^{3+} is stable and goethite precipitates. Therefore, the hydrated Red clay has no mineral drive for oxidation reactions with DIW and the antibacterial action ends.

Role of reactive oxygen species

Morrison *et al.* (2016) presented analysis of the antibacterial mechanism and the role of reduced Fe in the OMT antibacterial clay. Reactive oxygen species (ROS) are formed during the oxidation of pyrite (Schoonen *et al.*, 2010) following the well known Fenton reaction series (Fenton, 1894). Either dissolved
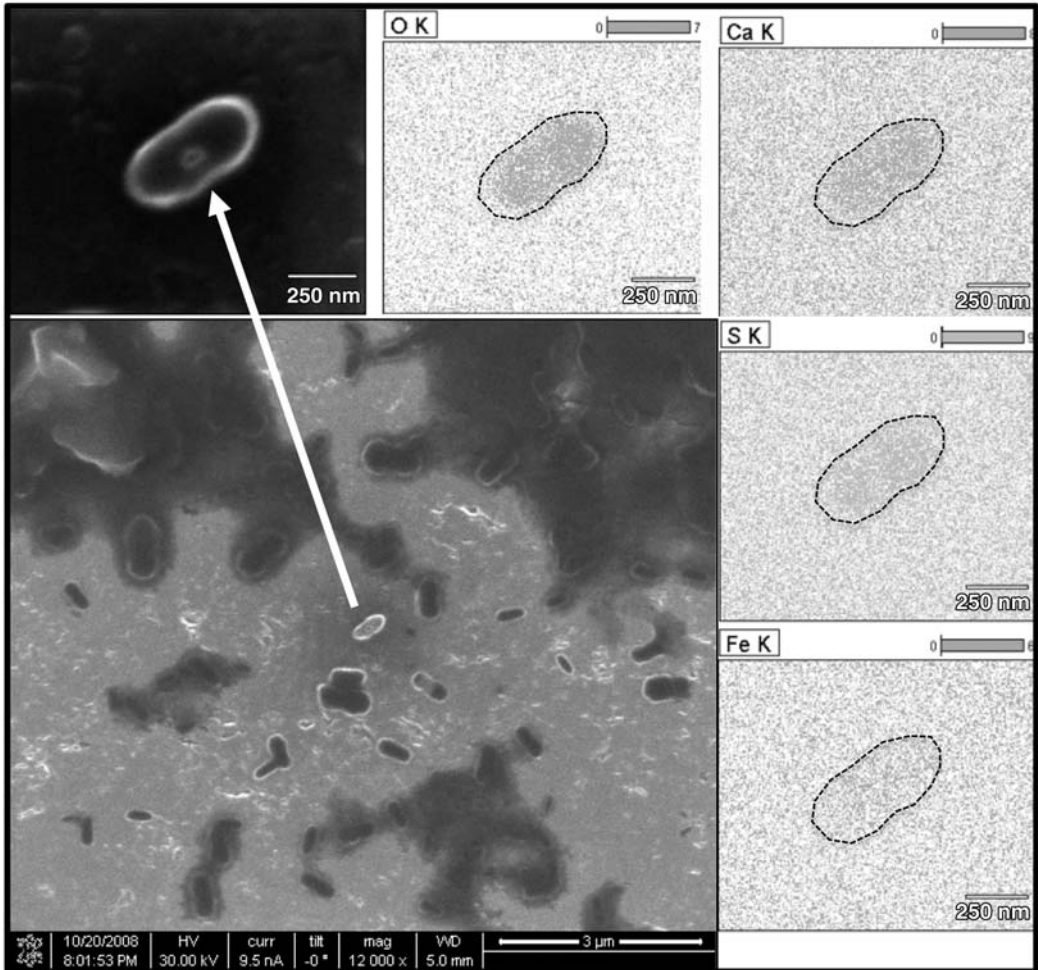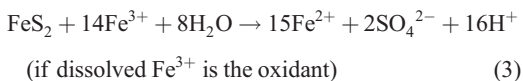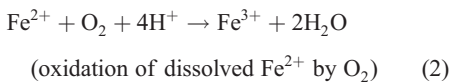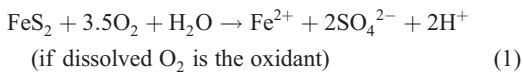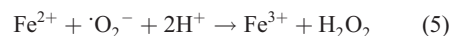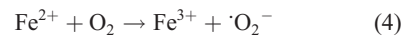
FIG. 11. SEM and energy dispersive X-ray maps showing microbe-shaped bodies, in the OMT Blue clay, which concentrate O, Ca, S and Fe. These are interpreted as environmental microbes which metabolize and concentrate Fe^{2+}.

O_2 or Fe^{3+} can oxidize sulfur in pyrite when hydrated with DIW (Rimstidt & Vaughan, 2003):

$$FeS_2 + 3.5O_2 + H_2O \rightarrow Fe^{2+} + 2SO_4^{2-} + 2H^+$$

(if dissolved O_2 is the oxidant)   (1)

$$Fe^{2+} + O_2 + 4H^+ \rightarrow Fe^{3+} + 2H_2O$$

(oxidation of dissolved Fe^{2+} by O_2)   (2)

$$FeS_2 + 14Fe^{3+} + 8H_2O \rightarrow 15Fe^{2+} + 2SO_4^{2-} + 16H^+$$

(if dissolved Fe^{3+} is the oxidant)   (3)

During the dissolution of pyrite, intermediate reactions produce ROS-containing radical molecules (Friedlander *et al.*, 2015) or ferryl ion (FeO^{2+}; Barbusinski, 2009), both oxidants that are destructive to biomolecules:

$$Fe^{2+} + O_2 \rightarrow Fe^{3+} + \cdot O_2^-$$ (4)

$$Fe^{2+} + \cdot O_2^- + 2H^+ \rightarrow Fe^{3+} + H_2O_2$$ (5)

$$Fe^{2+} + H_2O_2 \rightarrow Fe^{3+} + OH^- + \cdot OH$$ (6)

The reaction series 7 represents a stepwise one-electron reduction of dissolved oxygen (Prousek, 2007) as a reduced metal (*e.g.* Fe^{2+}) is oxidized:

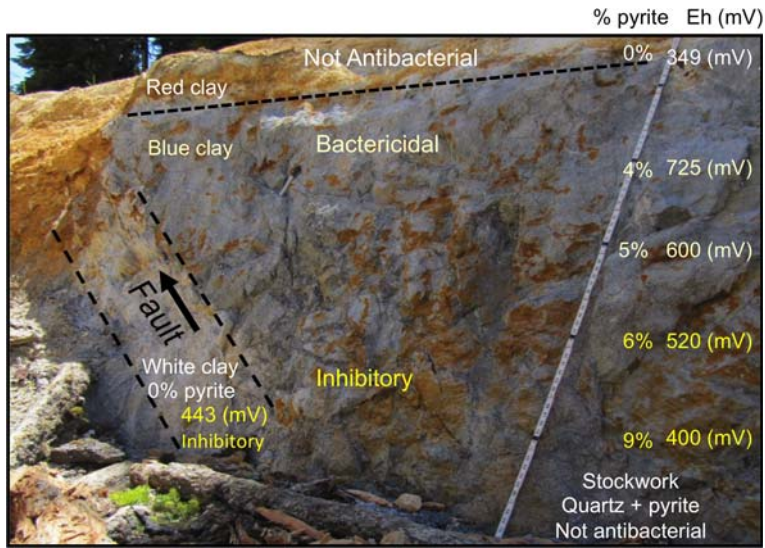$$O_2 \rightarrow \cdot O_2^- \rightarrow H_2O_2 \rightarrow \cdot OH \rightarrow H_2O$$ (7)

FIG. 12. Cross section sampled through the OMT Blue clay in the Open Pit reveals that the antibacterial effectiveness decreases with depth as the oxidation state of the hydrated clay decreases. The pyrite content increases with depth, but is negatively correlated with bactericide. Oxidation state is the dominant control on the antibacterial process.

Therefore, production of hydrogen peroxide (H_2O_2), a stable molecule, can be used as a proxy for the production of hydroxyl radical ($^{\bullet}$OH) (Cohn *et al.*, 2005), which is a species that has a very short existence (10^{-9} s half life), reacting within a few nanometers of where it forms (Winterbourn, 2008). Cohn *et al.* (2005) described a method using leuco-crystal violet and horseradish peroxidase to measure the production of H_2O_2 from minerals. Measurements of H_2O_2 produced by OMT clay suspensions show trends that correlate with metal solubility.

The antibacterial activity of the OMT clays was measured in outcrops across the entire deposit, using zone of inhibition testing as an indicator of bactericidal effectiveness. The diameter of growth inhibition (mm) was measured on 100 mg clay/mL suspensions of clay in disk diffusion wells (Fig. 8) and trends were observed as a function of pH (Fig. 13). Both the Gram-negative and Gram-positive model bacteria (*E. coli* and *S. epidermidis*, respectively) showed the greatest bactericide at low pH (<5), but no effect as the pH increased into the calcite stability region. Coincident with this pH increase, Morrison *et al.* (2016) observed a decrease in the concentration of Fe^{3+}, Fe^{2+} and Al^{3+}, the dominant aqueous metals in the leachate. Pourbaix stability diagrams for Fe-S-O and Al-O-H (at 25°C) were used to indicate the aqueous speciation of OMT clay suspensions relative to their antibacterial

effectiveness (Fig. 14). Only those clays buffering fluid pH and Eh in the stability fields for aqueous Fe^{2+} and Al^{3+} are antibacterial. Measurements of hydrogen peroxide (H_2O_2) followed the concentrations of the metals, decreasing from ~1500 µM at pH 2.5 to 0 µM at pH 5. *E. coli* cells are affected by H_2O_2 concentrations greater than 25 µM and ~100 µM is needed to achieve significant bacterial mortality (Hyslop *et al.*, 1995).

Using the production of H_2O_2 as an indicator of the presence (and reactivity) of dissolved Fe^{2+}, Morrison *et al.* (2016) evaluated the concentration of H_2O_2 in a time series for clay suspensions compared to aqueous leachates alone. The concentration of the clay (20 mg clay/mL) was the same as the leachate (20 mg clay/mL, equilibrated for 24 h, then separated). The results showed that the clay suspension generates ROS continuously over 24 h, whereas the aqueous leachate loses its ability to produce ROS in <1 h (data not shown). This points to the importance of the clay as a continuous source of reactants and in buffering the pH to conditions that keep Fe^{2+} stable and soluble. If Fe^{2+} is absorbed into the smectite interlayers it may be released slowly over an extended time promoting long-lasting antibacterial effects compared to metal solutions alone. To test this, Morrison (2015) saturated the non-antibacterial SWy-1 smectite with 1 M $FeCl_2$, and found that the addition of interlayer Fe^{2+} to the smectite made it antibacterial (data not shown).
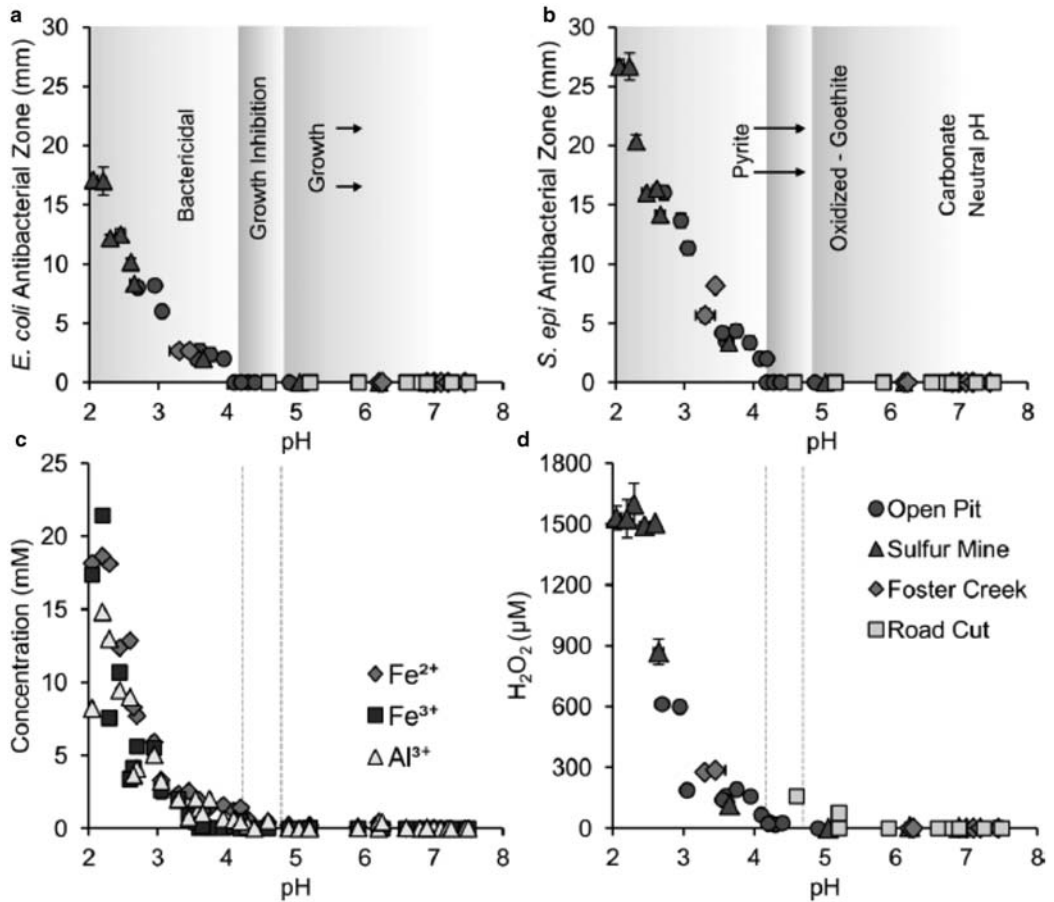
FIG. 13. Trends with pH in antibacterial effectiveness across the OMT deposit, indicated by zones of inhibition (mm) from clay suspensions (100 mg/mL): (a) Gram-negative *E. coli*; (b) Gram-positive *S. epidermidis*; (c) major metals in solution; (d) hydrogen peroxide (from Morrison *et al*., 2016; open access).

BIOIMAGING

TEM

Critical point drying of bacteria (see Morrison *et al*., 2014) in time series after incubation (37°C) with aqueous leachates of the OMT Blue clay, allowed TEM imaging of the *E. coli* cells as they responded to the hydrated clay components (Fig. 15). After 1 h, small black precipitates that were initially on the cell membrane, migrate to the polar ends of the *E. coli* cells (Williams *et al*., 2011). However, after 24 h, these black precipitates have entered the cell interior, and damage is clearly seen by the formation of voids (white holes), which may be artifacts of the cell microtoming through phosphate granules that pluck out. Such

granules are produced as phosphate anions and are used and stored for regulation of cation transport across the cell membrane (Schmidt *et al*., 2006).

Synchrotron: Scanning Transmission X-ray Microscopy

Bioimaging of the interaction of *E. coli* in suspensions of the OMT clay and leachate was performed at the Advanced Light Source in Berkeley, California (Lawrence Berkeley National Laboratory, USA; Morrison *et al*., 2016). Using STXM maps of the bacteria in clay suspensions (in silicon nitride cells), chemical changes in the bacteria and suspensions were monitored over time (12 h). Near-edge X-ray absorption
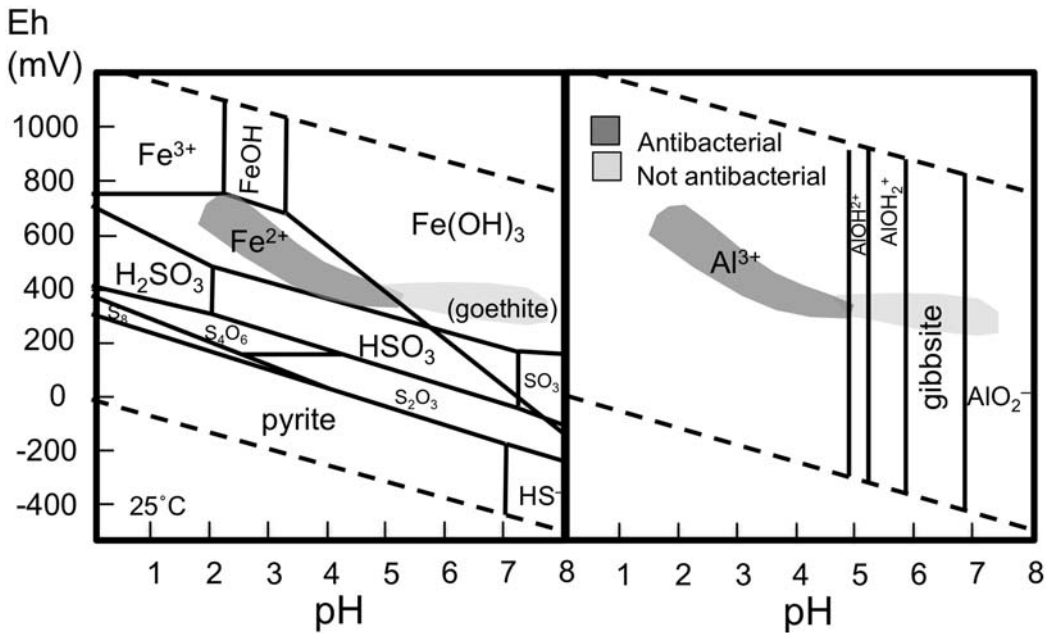
FIG. 14. Eh-pH stability plots at 25°C for aqueous: (a) Fe-S-O (modified from Morrison, 2015) and (b) Al-O (data from Takeno, 2005) showing the range of antibacterial and non-antibacterial clay suspensions from the OMT alteration assemblages.

fine structure spectra (NEXAFS) were collected in time series that indicate I-S in association with *E. coli* (Fig. 16a). The Fe spectra indicate Fe^{2+}-rich clays (Fig. 16b). After 12 h (Fig. 16c), Fe^{2+} is attracted to *E. coli* (green) leaving the solution enriched in Fe^{3+} (red). This makes sense because *E. coli* utilize reduced Fe in their metabolism, while Fe^{3+} must be reduced by siderophores in order to be transported across the cell membrane (Kammler *et al*., 1993; Lemire *et al*., 2013). The important finding was that Fe^{2+} dominates at the cell membrane and produces ROS that may damage membranes.

Nano-Secondary Ion Mass Spectrometry (SIMS)

Using Nano-secondary ion mass spectrometry (National SIMS Facility at Arizona State University, USA), the *E. coli* reacted with OMT clay (24 h) were further analysed chemically in their glutaraldehyde-fixed form (Orphan & House, 2009), mounted on Si wafers. Aqueous Fe and Al dominate the OMT Blue clay leachate (Table 2); therefore, we investigated their potential uptake and spatial distribution in *E. coli*. Use of a Cs^+ primary ion beam facilitates the spatial resolution needed to study elemental distributions on a

scale of <50 nm; therefore, the negative secondary ion emissions from a Cs^+ bombardment of the cells was measured using a 1 pA current and 10 µm rastered area. Aluminium (measured at mass 54 for $^{27}Al_2^-$) dominated on the cell membranes, while Fe (measured at mass 72 for FeO^-) dominated in the intracellular region (Fig. 17). This was the first confirmation that Al played a role in damage to the *E. coli* cell membranes, in addition to the Fe^{2+}, shown by STXM to be attracted to the membrane.

Morrison *et al*. (2016) used genotoxicity testing to further evaluate the role of the individual metals in reactions that affected different bacterial proteins. Aqueous Al^{3+} caused the most damage to cell membrane proteins, compared to intracellular proteins, whereas Fe^{2+} caused the most damage to DNA. This supported previous observations of damage to both linear and circular DNA indicated by PCR assays of the OMT leachate (Williams *et al*., 2011).

Electron Energy Loss Spectra (EELS)

One last piece of evidence that shed light on the order of chemical events in the antibacterial mechanism of the OMT Blue clay was from TEM electron
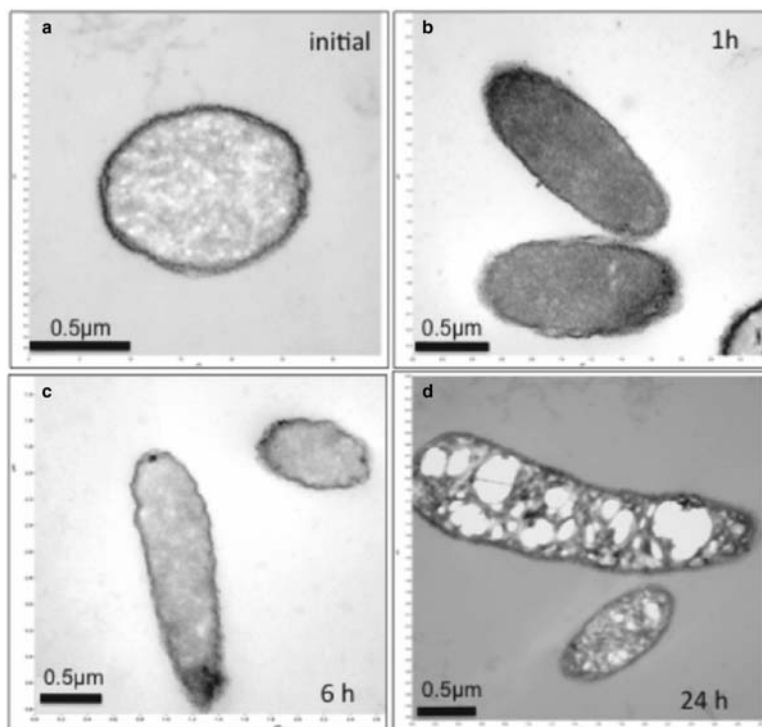
F_{IG}. 15. Time series over 24 h of *E. coli* reacted with OMT leachate (37°C) showing morphological changes occurring during the cell destruction (reprinted with permission from Williams *et al.* (2011). Copyright 2011, the American chemical Society).

energy loss analysis (EEL) of the small black particles found inside the *E. coli* upon cell death (Fig. 15). The EEL image (Fig. 18) shows those electron-dense areas as white spots, and Morrison *et al.* (2014) compared the Fe^{2+} and Fe^{3+} energy spectra of the white spots to adjacent areas within a single bacterium. It confirmed that the spots were Fe^{3+}, likely precipitates of Fe-oxides or hydroxides indicating oxidation of the Fe^{2+} that entered through the cell membrane.

The conclusion supports observations made by others (Gutteridge *et al.*, 1985; Zatta *et al.*, 2002) that Al and Fe act together to enhance damage to bacteria. The role of the Al^{3+}, derived from dissolution of aluminosilicates in the clay assemblage (plagio-clase, smectite), is to damage proteins in the cell membrane, which may disrupt the metabolic mechanisms that regulate the uptake of Fe^{2+}. Uncontrolled transport of large amounts of Fe^{2+} across the membrane can be toxic (Repine *et al.*, 1981; Keyer & Imlay, 1996; Andrews *et al.*, 2003). Evidence for production of ROS was shown by the large amount of hydrogen peroxide generated by the Fe^{2+} in the

aqueous leachates (Fig. 13). However, the cellular destruction (Fig. 15d) is by intracellular Fe^{2+} oxidation reactions, because hydroxyl radicals do not exist long enough to migrate more than a few nanometers before reacting with biomolecules (Winterbourn, 2008). The distribution of intracellular Fe^{3+}-oxide precipitates is evidence for reactions that occurred within the cell, producing hydroxyl radical damage to proteins (Repine *et al.* 1981; Morrison *et al.*, 2016).

COLOMBIAN LACUSTRINE CLAY

Not all antibacterial clays are from hydrothermal environments, where transition metals are abundant and play a dominant role in the toxicity. Recently, Londoño & Williams (2016) studied a lacustrine clay (Hoorn, 1994) from the Colombian Amazon (AMZ) near Araracuara, that is dominated by kaolins and smectite, with very little Fe content in the aqueous leachate (Table 2). This clay shows significant dissolution textures (Londoño & Williams, 2016), in moderately disordered kaolinite (Hinkley Index 0.8).
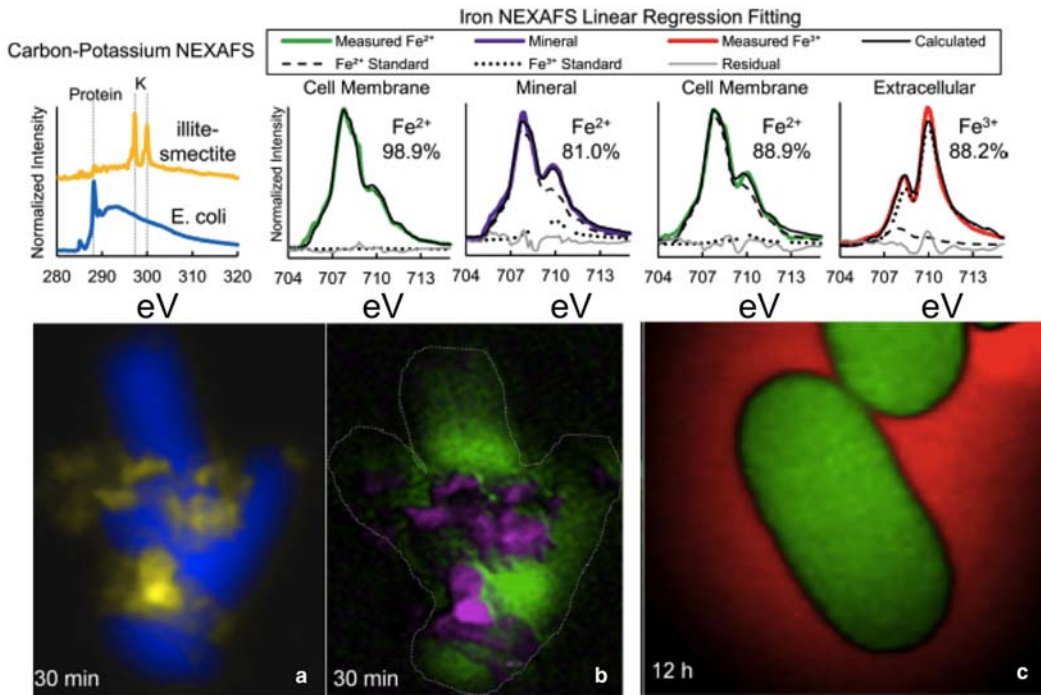
FIG. 16. Near-edge X-ray absorption fine structure mapping of Fe in OMT Blue clay suspensions with *E. coli* (modified from Morrison *et al*., 2016). (a) I-S (yellow) is indicated by K content on *E. coli* (blue) after 30 min; (b) Fe^{2+}-dominant clays (purple) on Fe^{2+}-enriched cell membranes (green); (c) Fe^{2+} is attracted preferentially to cells (green) after 12 h, leaving Fe^{3+}-enriched fluid (red).
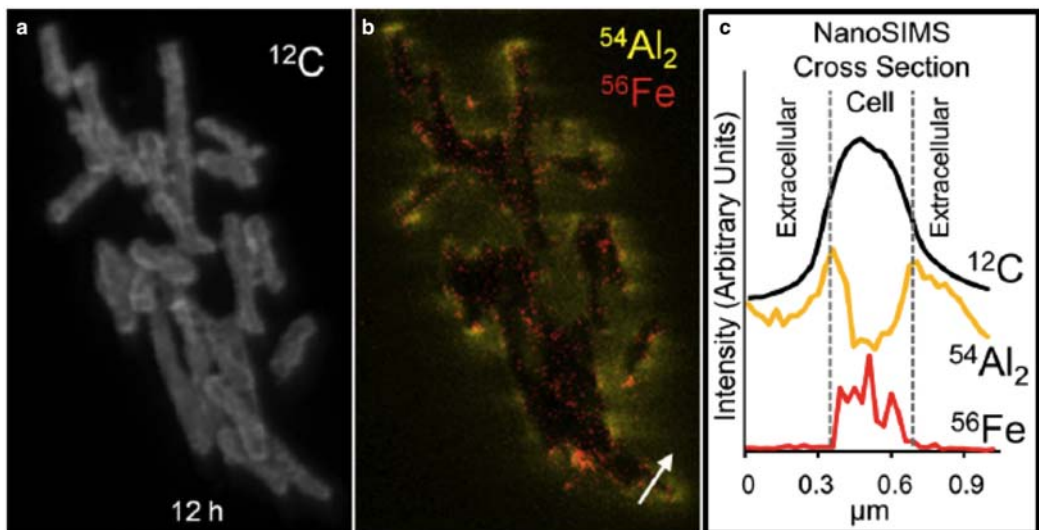

FIG. 17. Nano-SIMS showing: (a) a cluster of *E. coli* treated with OMT leachate; (b) Al (yellow) and Fe (red) distributions in the *E. coli*; (c) cross section across a single cell (white arrow in b) showing elevated Al on cell membranes and intracellular Fe (modified from Morrison *et al*., 2016).
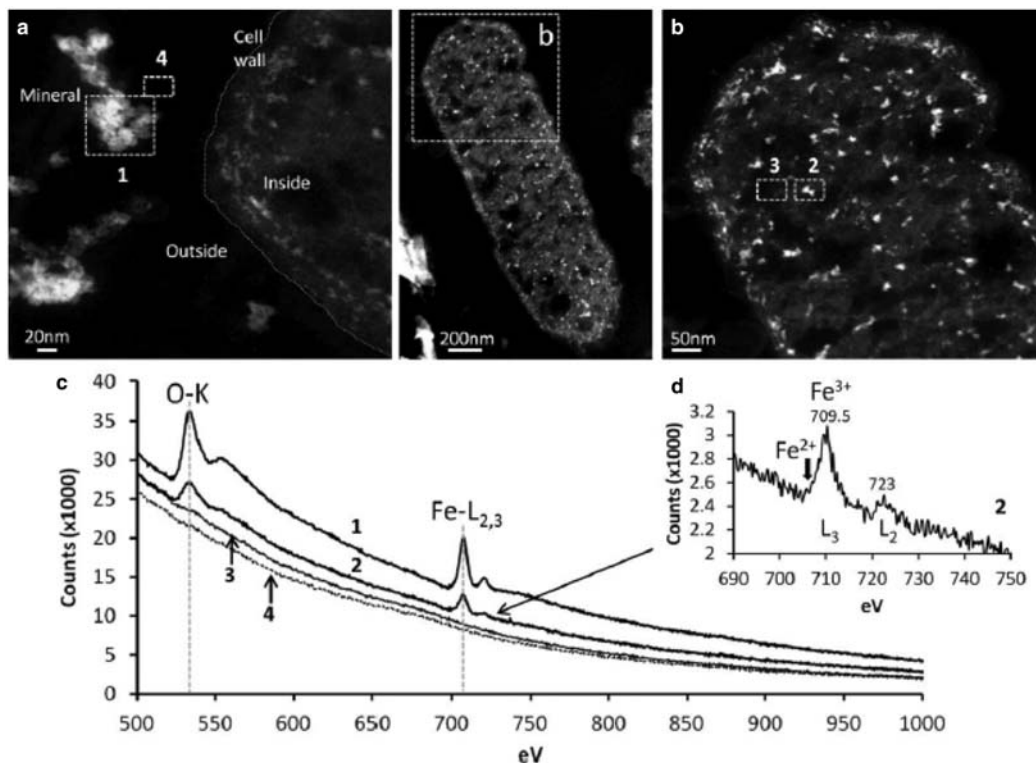
FIG. 18. Electron energy loss study of the opaque precipitates observed in *E.coli* reacted for 24 h with OMT leachate (from Morrison *et al.*, 2014): (a) areas 1 and 4 compare mineral to no mineral; (b) close-up of electron-dense area 2, compared to 3 background; (c) EEL spectra for areas 1–4; and (d) close up of energy spectra indicating Fe^{3+} precipitates.

The AMZ is not as effective as OMT at killing the model bacteria tested (*E. coli* and *B. subtilis*), but at higher concentrations (300 mg clay/mL) it is bactericidal. Interestingly, the aqueous leachate of the clay is not antibacterial, rather physical proximity of the clay to the cell membrane is required. We tested the physical attraction between the clay and *E. coli* (model Gram-negative bacteria) and *B. subtilis*, (model Gram-positive bacteria). The zeta potential (Fig. 19) was negative for all surfaces over the pH range of ∼3 to 9, indicating that there should be a repulsion between the minerals and bacteria. At the pH (∼4.6) buffered naturally by the clay there was a repulsion greater than 17 mV between the clay and the bacteria; therefore one may conclude that the negative surface potentials affect the competition for cations that could be nutrients or toxins to the bacteria.

Unlike the OMT Blue antibacterial clay, when the AMZ is reacted with *E. coli*, the bacteria lose P and Mg, and gain Al. There is no other significant exchange of elements, so initially we thought that the

clay was absorbing nutrients from the bacteria, causing their population decline (Londoño & Williams, 2016). However, addition of excess P and Mg to the growth media did not re-establish bacterial growth; the bacteria died even in the presence of sufficient nutrients. This
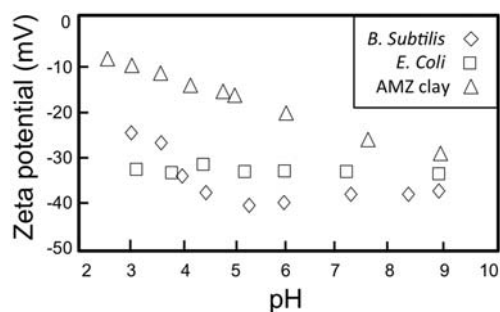

FIG. 19. Zeta potential of two model bacterial pathogens compared to the AMZ clay suspension in DIW (equilibrated for 24 h).
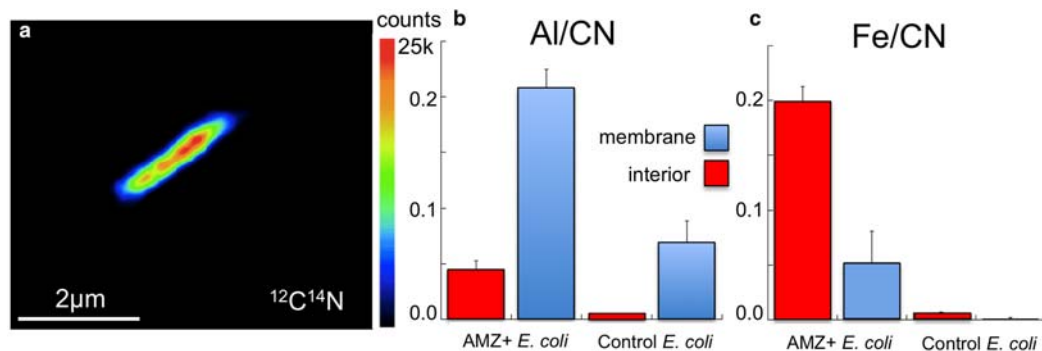
FIG. 20. NanoSIMS measurement of Al and Fe distribution in *E. coli* treated with AMZ clay. Negative ion counts of: (a) matrix CN^-; (b) Al/CN ratios in the AMZ-treated *E. coli* compared to untreated control; and (c) Fe/CN ratios accumulated over membrane *vs.* interior.

led to the hypothesis that Al was damaging these cell membranes, releasing P from phospholipids in the cell membrane (Londoño *et al.*, 2017).

In order to evaluate the potential uptake of Al by the bacteria reacted with AMZ, NanoSIMS ion imaging of *E. coli* reacted with AMZ was performed similar to the previous study on OMT Blue clay. Here we normalized the elements of interest to the matrix (CN). To avoid a potential topographic effect of the ion distribution from the non-flat, cylindrically shaped bacteria, instead of taking cross sections we rastered (10 μm^2) over the entire cell and collected depth-profiles through the cells (*e.g.* Orphan & House, 2009), from the top membrane of the bacteria (mounted on a Si wafer), through the interior and into the lower membrane (Fig. 20). *WinImage*™ software on the Cameca 50 L NanoSIMS allows users to select regions of interest and accumulate (integrate) the pixels in a volume under that region. Therefore, we can evaluate qualitatively the counts of ions coming from the cell interior *vs.* the cell membranes. Quantification is not possible without measuring a standard of each element within the same matrix. While CN molecules are major components of bacterial membranes and intracellular components, their molecular composition varies significantly; therefore, the sputtering rate (release of secondary ions) may change as a function of the matrix composition (Wilson *et al.*, 1989). Nonetheless, by normalizing each ionic species of interest to the major component of the matrix, one can evaluate the relative distribution of elements of interest.

Results from *E. coli* cells reacted with AMZ clay were compared to control *E. coli* grown without clay, and clear differences in the cell compositions were observed (Fig. 20). There is an increase in the Al/CN

ratio of the bacterial membrane compared to the control, and slightly higher Al/CN in the cell interior than the control. Al^{3+} is not known to penetrate living bacterial membranes without a chelator that promotes its transport into the cell (Guida *et al.*, 1991; Williams, 1999). However, if the membranes are damaged by toxic Al concentrations, as indicated by the release of P from the bacteria, then Al may have entered the cell interior post-mortem.

The Fe/CN ratios show a 20-fold increase in the intracellular Fe of the AMZ-treated *E. coli* over the untreated control *E. coli*. This is surprising because Fe is not one of the major transition metals of the aqueous leachates of the AMZ clays, yet it does show elevated concentrations in AMZ leached with growth media (LB), along with Cu, Zn and Mn (Londoño *et al.*, 2017). This points to a role of ionic strength in the sequestration of toxic metals from clays. Individually, the metals are not antibacterial at the pH 4.6 buffered by the clay. However, combined, they were shown to be antibacterial. NanoSIMS analyses of Cu/CN showed no significant difference between the AMZ-reacted *E. coli* and the control due to low ionization of the negative secondary Cu ions.

FUTURE MEDICAL APPLICATIONS

At this point, research on the specific minerals, chemical conditions, and mechanisms by which natural clays kill human pathogens has implicated the important role of soluble metals in the process, and the equally important role of the clay minerals in buffering aqueous conditions to keep metals in solution long enough for oxidation reactions to impact the bacterial defenses. The next critical step is to evaluate the effect

of these clays on skin cells, both *in vitro* and *in vivo*. While mM levels of hydrogen peroxide indicate significant production of ROS during the oxidation of soluble metals, skin cells have their own supply of oxygen through blood vessels that may help to maintain the cellular functions in the presence of elevated aqueous ROS (Hyslop *et al*., 1995). The fact that the bacteria are 'planktonic' (floating organisms in water), rather than integrated into a living organ makes them more vulnerable to the kind of attack demonstrated by the antibacterial clays described. Therefore, testing of the clay effect on pathogenic biofilms is a priority.

The topical application of natural antibacterial clays to wounds comes with the inherent risk of nanoparticulate silicates that can potentially migrate into the bloodstream, where cases of thrombosis (lung, brain) have been documented (Baker *et al*., 2007, Lawton *et al*., 2009). This is true of any particulate material, but the risks must be assessed. In general, the salinity of the clay poultices will cause aggregation of nanoparticles that could render them large enough to be unable to penetrate the vascular system. Alternatively, efforts can be made to eliminate the nanoparticulate fraction from the clay before application, which could be done by gravimetric settling of the coarser (>0.1 μm fraction) clays through water, then siphoning off the suspended fine particles.

Note that daily internal use of natural clays for long periods of time can be hazardous to health. Clay minerals have an enormous surface area that interacts with the aqueous environment. The antibacterial clays studied here are thought to have formed in hydrothermal environments where volcanogenic waters may carry and incorporate metals into the minerals that precipitate. Associated with hydrothermal systems are elements that are toxic in low doses (*e.g.* As, Hg) if they are in bioavailable forms, and can easily adsorb to clay mineral surfaces, especially in interlayers, where they may be preserved until hydration for a medical use. While the use of antibacterial clays for topical wound care may be tolerated in the short term, the long-term ingestion of clays, often promoted online by unregulated Neutraceutical companies, could lead to accumulation of bioavailable toxins in the body.

The identification of volcanogenic hydrothermal alteration assemblages as a primary depositional environment for clays with antibacterial properties should lead to more discoveries of antibacterial clay deposits worldwide (Londoño & Williams, 2016; Morrison *et al*., 2016). While this could provide a new economic outlet for such reserves, the application to human health requires further study to understand interactions with human tissues, and potential side effects. Nonetheless, by evaluating antibacterial clays and mimicking the natural geochemical processes (geomimicry) recognized and utilized by our ancestors, we may discover new solutions for treating antibiotic-resistant bacteria.

REFERENCES

Amyes S., Miles R.S., Thomson C.J. & Tillotson G. (1996) *Antimicrobial Chemotherapy.* CRC Press, Taylor & Francis Group, Boca Raton, Florida, USA, 72 pp.

Andrews S.C., Robinson A.K. & Francisco R.-Q. (2003) Bacterial iron homeostasis. *FEMS Microbiology Reviews*, **27**, 215–237.

Bacon C.R. & Nathenson M. (1996) *Geothermal resources in the Crater Lake area, Oregon.* U.S. Geological Survey Open-File Report, 96-663.

Baker S.E., Sawvel A.M., Zheng N. & Stucky G.D. (2007) Controlling bioprocesses with inorganic surfaces: Layered clay hemostatic agents. *Chemistry of Materials*, **19**, 4390–4392.

Barbusinski K. (2009) Fenton reaction: Controversy concerning the chemistry. *Ecological Chemistry and Engineering*, **16**, 347–358.

Bauer A.W., Kirby W.M.M., Sherris J.C. & Turck M. (1966) Antibiotic susceptibility testing by a standardized single disk method. *American Journal of Clinical Pathology*, **45**, 493–496.

Carretero M.I., Gomes C.S.F. & Tateo F. (2013) Clays and human health. Pp. 717–741 in: *Handbook of Clay Science*, 2nd edition (F. Bergaya & G. Lagaly, editors). Developments in Clay Science 5, Elsevier, Amsterdam.

CLSI, Clinical Laboratory Standards Institute (2015) *Methods for Dilution Antimicrobial Susceptibility Tests for Bacteria That Grow Aerobically; Approved Standard – tenth edition.* Wayne, Pennsylvania, USA, CLSI document M07-A10, **35**, pp. 1–45.

Cohn C.A., Pak A., Strongin D. & Schoonen M.A. (2005) Quantifying hydrogen peroxide in iron containing solutions using leuco-crystal violet. *Geochemical Transactions*, **6**, 47–51.

Eberl D.D. (2003) *User's guide to RockJock; A program for determining quantitative mineralogy from powder X-ray diffraction data.* U.S. Geological Survey Open-File Rep. 2003-78, 47 pp.

Fenton H.J.H. (1894) Oxidation of tartaric acid in presence of iron. *Journal of Chemical Society Transactions*, **65**, 899–911.

Ferrell Jr. R.E. (2008) Medicinal clay and spiritual healing. *Clays and Clay Minerals*, **56**, 751–760.

Foster J.W. and Woodruff H.B. (2010) Antibiotic substances produced by bacteria. *Annals of the New York Academy of Science*, **2013**, 125–136.

Friedlander L.R., Puri N., Schoonen M.A.A. & Karzai W. (2015) The effect of pyrite on *Escherichia coli* in water: proof-of-concept for the elimination of waterborne bacteria by reactive minerals. *Journal of Water Health*, **13.1**, 42–53.

George K.M., Chatterjee D., Gunawardana G., Welty D., Hayman J., Lee R. & Small P.L.C. (1999) Mycolactone: a polyketide toxin from *Mycobacterium ulcerans* required for virulence. *Science*, **283**, 854–7.

Guida L., Saidi Z., Hughes M. & Poole R. (1991) Aluminum toxicity and binding to *Escherichia coli*. *Archives of Microbiology*, **156**, 507–512.

Gutteridge J.M., Quinlan G.J., Clark I. & Halliwell B. (1985) Aluminium salts accelerate peroxidation of membrane lipids stimulated by iron salts. *Biochimica et Biophysica Acta – Lipids and Lipid Metabolism*, **835**, 441–447.

Haydel S.E., Remenih C.M. & Williams L.B. (2008) Broad-spectrum in vitro antibacterial activities of clay minerals against antibiotic-susceptible and antibiotic-resistant bacterial pathogens. *Journal of Antimicrobial Chemotherapy*, **61**, 353–361.

Hoogerheide J.C. (1944) Antibiotic substances produced by soil bacteria. *Botanical Review*, **10**, 599–638.

Hoorn C. (1994) Fluvial palaeoenvironments in the intracratonic Amazonas Basin (early Miocene–early Middle Miocene, Colombia). *Palaeogeography & Palaeoclimate*, **109**, 1–54.

Hyslop P.A., Hinshaw D.B., Scraufstatter I.U., Cochrane C.G., Kunz S. & Vosbeck K. (1995) Hydrogen peroxide as a potent bacteriostatic antibiotic: implications for host defense. *Free Radical Biology and Medicine*, **19**, 31–37.

Kammler M., Schön C. & Hantke K. (1993) Characterization of the ferrous iron uptake system of *Escherichia coli*. *Journal of Bacteriology*, **175**, 6212–6219.

Keyer K. & Imlay J.A. (1996) Superoxide accelerates DNA-damage by elevating free-iron levels. *Proceedings of the National Academy of Sciences, USA*, **193**, 13635–13649.

Kibanova D., Nieto-Camacho A. & Cervini-Silva J. (2009) Lipid peroxidation induced by expandable clay minerals. *Environmental Science & Technology*, **43**, 7550–7555.

King G.M., Weber C.F., Ohta H., Sato Y. & Nanba K. (2008) Molecular survey and activities of carbon monoxide oxidizing bacteria on volcanic deposits in Miyake-jima, Japan. *Microbes & Environments*, **23**, 299–305.

Konhauser K.O. & Urrutia M.M. (1999) Bacterial clay authigenesis: a common biogeochemical process. *Chemical Geology*, **161**, 399–413.

Kvitko B.H., Goodyear A., Propst K.L., Dow S.W. & Schweizer H.P. (2012) Burkholderia pseudomallei known siderophores and Hemin uptake are dispensable for lethal Murine Melioidosis. *Public Library of Science: Neglected Tropical Diseases*, **6**, e1715.

Lawton G., Granville-Chapman J. & Parker P.J. (2009) Novel hemostatic dressings. *Journal of the Royal Army Medical Corps*, **155**, 309–314.

Lemire J.A., Harrison J.J. & Turner R.J. (2013) Antimicrobial activity of metals: mechanisms, molecular targets and applications. *Nature Reviews* **11**, 371–384.

Londoño S.C. & Williams L.B. (2016) Unraveling the antibacterial mode of action of a clay from the Colombian Amazon. *Environmental Geochemistry & Health*, **38**, 363–379.

Londoño S.C., Hartnett H.H. & Williams L.B. (2017) The antibacterial activity of aluminum in clay from the Colombian Amazon. *Environmental Science & Technology.* doi: 10.1021/acs.est.6b04670.

Marsollier L., Rober R., Aubry J., Saint André J-P., Kouakou H., Legras P., Manceau A.-L., Mahaza C. & Carbonnelle B. (2002) Aquatic insects as a vector for Mycobacterium ulcerans. *Applied & Environmental Microbiology*, **68**, 4623–4628.

Moore D.M. & Reynolds R.C. (1997) *X-ray Diffraction and the Identification and Analysis of Clay Minerals*, 2nd edition. Oxford University Press, New York.

Morrison K.D. (2015) Unearthing the antibacterial activity of a natural clay deposit. PhD dissertation, Arizona State University, Arizona, USA, 157 pp.

Morrison K.D., Underwood J.C., Metge D.W., Eberl D.D. & Williams, L.B. (2014) Mineralogical variables that control the antibacterial effectiveness of a natural clay deposit. *Environmental Geochemistry & Health*, **36**, 613–631.

Morrison K.D., Misra R. & Williams L.B. (2016) Unearthing the antibacterial mechanism of medicinal clay: A geochemical approach to combating antibiotic resistance. *Nature Scientific Reports*, **5**, 19043; doi: 10.1038/srep19043.

Nies D.H. (1999) Microbial heavy-metal resistance. *Applied Microbiology & Biotechnology*, **51**, 730–750.

Orphan V.J. & House C.H. (2009) Geobiological investigations using secondary ion mass spectrometry: microanalysis of extant and paleo-microbial processes. *Geobiology*, **7**, 360–372.

Portaels F., Meyers W.M., Ablordey A., Castro A.G., Chemlal K. (2008) First cultivation and characterization of *Mycobacterium ulcerans* from the environment. *Public Library of Science Neglected Tropical Diseases* **2**, e178. doi: 10.1371/journal.pntd.0000178.

Prousek J. (2007) Fenton chemistry in biology and medicine. *Pure & Applied Chemistry*, **79**, 2325–2338.

Repine J.E., Fox R.B. & Berger E.M. (1981) Hydrogen peroxide kills *Staphylococcus aureus* by reacting with *Staphylococcal* iron to form hydroxyl radicals. *Journal of Biological Chemistry*, **256**, 7094–7096.

Rimstidt J.D. & Vaughan D.J. (2003) Pyrite oxidation: A state-of-the-art assessment of the reaction mechanism. *Geochimica et Cosmochimica Acta*, **67**, 873–880.

Schmidt D., Jiang Q. & McKinnon R. (2006) Phospholipids and the origin of cationic gating charges in voltage sensors. *Nature*, **444**, 775–779.

Schoonen M.A.A., Harrington A.D., Laffers R. and Strongin D.R. (2010) Role of hydrogen peroxide and hydroxyl radical in pyrite oxidation by molecular oxygen. *Geochimica et Cosmochimica Acta*, **74**, 4971–4987.

Takeno N. (2005) *Atlas of Eh-pH diagrams: Intercomparison of thermodynamic databases.* Geological Survey of Japan Open File Report No. 419, 285 pp.

Vermeer D.E. & Ferrell Jr, R.E. (1985) Nigerian geophagical clay: A traditional antidiarrheal pharmaceutical. *Science*, **227**, 634–636.

Weber C.F. & King G.M. (2010) Quantification of Burkholderia coxL genes in Hawaiian volcanic deposits. *Applied Environmental Microbiology*, **76**, 2212–2217.

Wei J.-C., Yen Y.-T., Su H.-L. & Lin J.-J. (2011) Inhibition of bacterial growth by the exfoliated clays and observation of physical capturing mechanism. *The Journal of Physical Chemistry C*, **115**, 18770–18775.

WHO, World Health Organization (2008) *Buruli ulcer disease (Mycobacterium ulcerans infection)*. World Health Organization. http://www.who.int/mediacentre/factsheets/fs199/en/

Williams R.J.P. (1999) What is wrong with aluminum? *Journal of Inorganic Biochemistry*, **76**, 81–88.

Williams L.B. & Haydel S.E. (2010) Evaluation of the medicinal use of clay minerals as antibacterial agents. *International Geology Review*, **52**, 745–770.

Williams L.B. & Hillier S. (2014) Kaolins and health: from first grade to first aid. *Elements*, **10**, 207–211.

Williams L.B., Holland M., Eberl D.D., Brunet T. & Brunet de Courssou L. (2004) Killer clays! Natural antibacterial clay minerals. *Mineralogical Society Bulletin*, **139**, 3–8.

Williams L.B., Haydel S.E., Giese R.F. & Eberl D.D. (2008) Chemical and mineralogical characteristics of French green clays used for healing. *Clays and Clay Minerals*, **56**, 437–452.

Williams L.B., Metge D.W., Eberl D.D., Harvey R.W., Turner A.G., Prapaipong P. & Poret-Peterson A.T. (2011) What makes natural clays antibacterial? *Environmental Science & Technology*, **45**, 3768–3773.

Wilson M.J. (2003) Clay mineralogical and related characteristics of geophagic materials. *Journal of Chemical Ecology*, **29**, 1525–1547.

Wilson R.G., Stevie F.A. & Magee C.W. (1989) *Secondary Ion Mass Spectrometry: A Practical Handbook for Depth Profiling and Bulk Impurity Analysis.* Wiley Interscience Publishers, New York, 384 pp.

Winterbourn C.C. (2008) Reconciling the chemistry and biology of reactive oxygen species. *Natural Chemical Biology*, **4**, 278–286.

Yokoyama S., Kuroda M. & Sato T. (2005) Atomic force microscopy study of montmorillonite dissolution under highly alkaline conditions. *Clays and Clay Minerals*, **53**, 147–154.

Young S.L. (2011) *Craving Earth.* Columbia University Press, New York, 228 pp.

Zatta P., Kiss T., Suwalsky M. & Berthon G. (2002) Aluminium (III) as a promoter of cellular oxidation. *Coordination Chemistry Reviews*, **228**, 271–284.

Zeelmaekers E., McCarty D. & Mystkowski K. (2009) *Sybilla* User Manual, Chevron ®ETC proprietary software. 16 pp.